J Mater Sci (2010) 45:5164–5170
DOI 10.1007/s10853-010-4551-z

Effects of transition metal oxide and Ni addition on the hydrogen-storage properties of Mg

Sung Nam Kwon · Daniel R. Mumm · Hye Ryoung Park · Myoung Youp Song

Received: 25 March 2010 / Accepted: 22 April 2010 / Published online: 11 May 2010

Abstract Mg-based hydrogen-storage materials with the compositions of Mg–10 wt%oxide (oxide = Cr_2O_3, Fe_2O_3, MnO, and SiO_2) and Mg–$x$$Fe_2O_3$–$y$Ni were prepared by reactive mechanical grinding (RMG). Taking into consideration the hydriding and dehydriding rates and the cost of materials, Fe_2O_3 prepared by spray conversion is an appropriate oxide additive to Mg. Mg–5 wt%Fe_2O_3–15 wt%Ni exhibited the best hydrogen-storage performance among the Mg–$x$$Fe_2O_3$–$y$Ni hydrogen materials. It stored 5.47 wt%H under 1.2 MPa H_2 for 60 min and released 5.42 wt%H under 0.1 MPa H_2 for 15 min at 593 K. The addition of Fe_2O_3 and Ni to Mg by the RMG shortens the diffusion distances through the reduction of the particle size of Mg. These additives are also considered to facilitate nucleation by creating many defects on the surface and in the interior of Mg. The added Fe_2O_3 and Ni themselves may also act as active sites for the nucleation. Ni forms the Mg_2Ni phase by a reaction with Mg, and Fe appears from the reduction of Fe_2O_3 by hydrogen after hydriding–dehydriding cycling.

S. N. Kwon
Department of Hydrogen and Fuel Cells Engineering, Specialized Graduate School, Chonbuk National University, 664-14 1ga Deogjindong Deogjingu, Jeonju 561-756, Republic of Korea

D. R. Mumm
Department of Chemical Engineering and Materials Science, University of California, Irvine, CA 92697-2575, USA

H. R. Park
Faculty of Applied Chemical Engineering, Chonnam National University, 300 Yongbongdong Bukgu, Gwangju 500-757, Republic of Korea

M. Y. Song (✉)
Division of Advanced Materials Engineering, Department of Hydrogen and Fuel Cells, Research Center of Advanced Materials Development, Engineering Research Institute, Chonbuk National University, 664-14 1ga Deogjindong Deogjingu, Jeonju 561-756, Republic of Korea
e-mail: songmy@jbnu.ac.kr

Introduction

In the forthcoming hydrogen economy, in which energy is stored and transported using hydrogen as an energy carrier for mobile applications (automobiles, aircraft, laptops, etc.), the development of efficient hydrogen-storage technology is the main challenge. Most of the research on this topic has focused on storing hydrogen safely in lightweight, compact, and high capacity systems. There are six storage methods currently being investigated: storing hydrogen as a gas, liquid hydrogen storage, the physisorption of hydrogen, and storing it in the form of metal hydrides and complex hydrides, and via chemical reactions [1].

Magnesium, one of the prospective hydrogen-storage materials, is able to store and release hydrogen gas. It has a high hydrogen-storage capacity of about 7.6 wt% and is abundant in the earth's crust. However, its hydrogen absorption and desorption kinetics are very slow and occur at very high temperatures (at least 350–400 °C and over a period of several hours).

One of the rate-controlling steps in the hydriding reaction of magnesium is the diffusion of hydrogen through the growing magnesium–hydride layer [2]. The hydriding kinetics of Mg can be improved, therefore, by a treatment such as mechanical alloying [2, 3], which can shorten diffusion distances by reducing the effective particle sizes of Mg.

The oxides are brittle, and thus they may be pulverized during mechanical grinding. The added oxides and/or their

pulverization during mechanical grinding may help the particles of magnesium become finer, leading to the increase in the hydriding and dehydriding rates of Mg. Oxides such as V_2O_5 [4], Cr_2O_3 [5, 6], Al_2O_3 [5], CeO_2 [5], CoO [7], Nb_2O_5 [8–12], and MgO [13] were added. Other compounds, such as FeF_3 [14] and organic additives [15, 16], were also added to Mg in order to improve reaction kinetics of Mg with hydrogen.

Song et al. [17] studied the hydriding and dehydriding properties of Mg–*x*wt%Ni ($x = 5$, 10, 25, and 55) mixtures mechanically alloyed under an argon atmosphere in a planetary mill. Mg–10 wt%Ni had the highest hydriding rate and the largest hydrogen-storage capacity, and showed a relatively high dehydriding rate. Bobet et al. [18] improved significantly the hydrogen-storage properties of both magnesium and Mg + 10 wt%Co, Ni, or Fe mixtures by mechanical alloying in H_2 (reactive mechanical grinding) for a short time (2 h). Ni and Fe [19], Palladium [20], and graphite [21, 22] were also added to enhance the hydriding and dehydriding rates of Mg. Berlouis et al. [23] investigated the effect of additives Ti, Pd, and Zr on the rate of hydrogen desorption from MgH_2, and reported that the presence of Pd and Zr enhanced dehydriding kinetics. Grigorova et al. [24] reported that the addition of an intermetallic compound $V_{0.855}Ti_{0.095}Fe_{0.05}$ by mechanical alloying in an inert medium improved significantly the hydriding kinetics of magnesium. Khrussanova et al. [25] obtained a nanocomposite 85 wt%Mg–15 wt%$Mg_2Ni_{0.8}Co_{0.2}$ by mechanical alloying in inert atmosphere, and explained its hydrogen sorption properties by the catalytic effect of the intermetallic $Mg_2Ni_{0.8}Co_{0.2}$, the existence of Ni and Co clusters on the surface, and the process of mechanical alloying.

In this work, Cr_2O_3, Fe_2O_3, MnO, and SiO_2 as oxides, and Ni as a transition metal element, were selected as additives to magnesium in order to improve the hydriding and dehydriding rates of magnesium. Mg-based samples in which transition metal oxides, and Fe_2O_3 along with Ni were added, were prepared by reactive mechanical grinding (RMG, mechanical milling under H_2) and its hydrogen-storage properties were measured. The effects of transition metal oxide and Ni addition on the hydrogen-storage properties of Mg were then investigated.

Experimental details

The starting materials were pure Mg powder (particle size 100–297 μm, purity 99%, Fluka), Fe_2O_3 (particle size 36 nm, prepared by spray conversion), Cr_2O_3 (particle size 18 nm, prepared by spray conversion), MnO (particle size 88–250 μm, purity 99%, Aldrich), SiO_2 (particle size 99 nm, prepared by spray conversion), and Ni (average particle size ~5 μm, purity 99.9%, Cerac). The preparation by spray conversion is explained in detail in reference [26]. The samples with the compositions of Mg–10 wt% oxide (oxide = Cr_2O_3, Fe_2O_3, MnO, and SiO_2) and Mg–*x*wt%Fe_2O_3–*y*wt%Ni were prepared. We designate the samples Mg–10 wt%oxide and Mg–*x*wt%Fe_2O_3–*y*wt%Ni as Mg–10oxide and Mg–xFe_2O_3–*y*Ni, respectively.

Reactive mechanical grinding (RMG) was done in a planetary ball mill (Planetary Mono Mill; Pulverisette 6, Fritsch). A mixture with the desired composition (total weight = 8 g) was mixed in a stainless-steel container (with 105 hardened steel balls, total weight = 360 g) sealed hermetically. The sample to ball weight ratio was 1/45. All sample handling was performed in a glove box under Ar in order to prevent oxidation. The disk revolution speed was 250 rpm. The mill container was then filled with high purity hydrogen gas (about 1.2 MPa). The RMG was performed by repeating milling (for 15 min) and cooling (for 5 min) eight times, resulting in total 2 h milling.

The quantity of hydrogen absorbed or desorbed was measured as a function of time by a volumetric method with a Sievert's type hydriding apparatus. X-ray diffraction (XRD) analysis was carried out for the as-milled powders and for the samples after hydriding–dehydriding cycling. The microstructures were observed by scanning electron microscopy (SEM).

Results and discussion

Figure 1 shows the variation of absorbed hydrogen quantity, H_a, versus time, t, curve at 593 K under 1.2 MPa H_2 with the activated Mg–10oxide sample. The percentage of absorbed hydrogen, H_a (wt%), is expressed with respect to the sample weight. The pure Mg absorbs a very small amount of hydrogen even for 60 min. On the other hand, the Mg–10oxide samples absorb hydrogen more rapidly and larger amounts of hydrogen than the pure Mg. The additions of Cr_2O_3 and Fe_2O_3 to Mg showed the strongest effects on the improvements in the hydriding rate and the hydrogen-storage capacity of Mg; the Mg–10Cr_2O_3 and the Mg–10Fe_2O_3 samples have the highest hydriding rates and the highest hydrogen-storage capacities. They have the hydriding rates of about 50 times (0.53, 0.47 wt%H/min for 10 min, respectively) and the hydrogen-storage capacities of about 13 times (5.72, 5.55 wt% for 60 min, respectively) as high as the pure Mg.

Figure 2 presents the variation of desorbed hydrogen quantity, H_d, versus time, t, curve at 593 K under 0.1 MPa H_2 with the activated Mg–10oxide sample. The percentage of desorbed hydrogen, H_d (wt%), is also expressed with respect to the sample weight. The pure Mg does not release hydrogen. The Mg–10SiO_2 sample releases

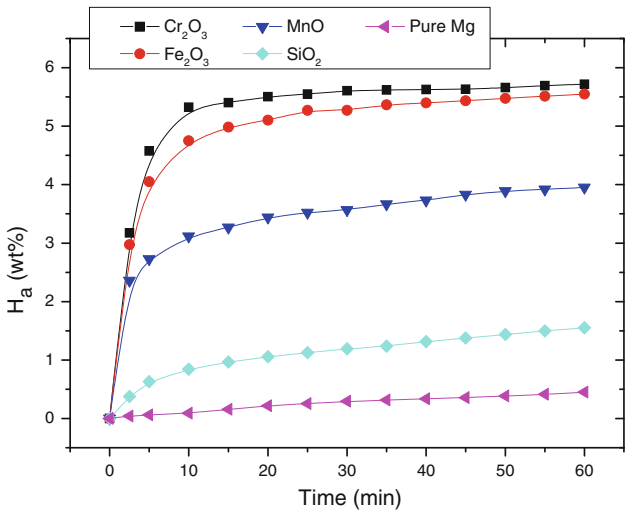

Fig. 1 Variation of absorbed hydrogen quantity, H_a, versus time, t, curve at 593 K under 12 bar H_2 with the activated Mg–10oxide sample

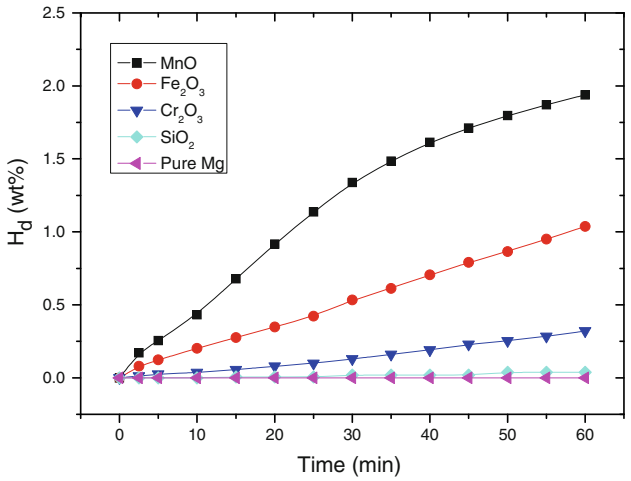

Fig. 2 Variation of desorbed hydrogen quantity, H_d, versus time, t, curve at 593 K under 1.0 bar H_2 with the activated Mg–10oxide sample

extremely small amount of hydrogen even for 60 min. The Mg–10MnO sample has the highest dehydriding rate followed in order by the Mg–10Fe_2O_3 and Mg–10Cr_2O_3 samples. The Mg–10MnO sample has the dehydriding rate of 0.044 wt%H/min for 30 min, and releases 1.94 wt%H for 60 min.

The microstructures are given in Fig. 3 for the pure Mg and the samples prepared by RMG with oxides Mg–10MnO, Mg–10Cr_2O_3, Mg–10SiO_2, and Mg–10Fe_2O_3. The particles of the pure Mg become larger after RMG than before RMG. This is because the Mg particles with good malleability and ductility are connected together, which is shown by their form of connected flat plates. On the other hand, oxide-added Mg particles have smaller particles than the pure Mg. The Mg–10MnO and Mg–10SiO_2 samples have also large particles with the form of flat plate like the pure particles, but with many defects and cracks. The Mg–10Cr_2O_3 sample has the smallest particles followed in order by the Mg–10Fe_2O_3, Mg–10MnO, and Mg–10SiO_2 samples. The Mg–10Cr_2O_3 sample has particle sizes similar to that of Mg–10Fe_2O_3 sample, and the Mg–10MnO sample has particle sizes similar to that of Mg–10SiO_2 sample. The above microstructures show that the addition of oxide to Mg facilitates pulverization of Mg, and thus increases the surface area of Mg particles, and creates a lot of defects and cracks. The defects can act as active sites for nucleation and the cracks can be used paths for the movement of hydrogen.

The XRD patterns of the Mg–10oxide samples dehydrided at 593 K for 3 h after activation are exhibited in Fig. 4. The pure Mg contains MgH_2 phase even after dehydriding, showing that the decomposition of MgH_2 phase is not completed due to very low dehydriding rate of magnesium hydride. On the other hand, the oxide-added samples do not reveal the MgH_2 phase, indicating that all the MgH_2 phase decomposed under the similar conditions. All the Fe_2O_3 in the Mg–10Fe_2O_3 was reduced to Fe. The oxides MnO and SiO_2 were partly reduced in the Mg–10MnO and Mg–10SiO_2, and the presence of Mn and Si were observed in these samples. The Cr_2O_3 in the Mg–10Cr_2O_3 was not reduced.

The oxide-added Mg particles had smaller particles than the pure Mg (Fig. 3), showing that the addition of the oxides to Mg by the RMG reduces the particle size of Mg. One of the rate-controlling steps in the hydriding reaction of magnesium is the diffusion of hydrogen through the growing magnesium–hydride layer [2], indicating that the hydriding kinetics of Mg can be improved by reducing the particle size of Mg. The order of high hydriding rate and high hydrogen-storage capacity, from Fig. 1, is Mg–10Cr_2O_3, Mg–10Fe_2O_3, Mg–10MnO, Mg–10SiO_2, and the pure Mg, which is very similar to the order of the particle size from Fig. 3. This shows that the addition of the oxides to Mg by the RMG shortens the diffusion distances through the reduction of the particle size of Mg and thus enhances the hydriding kinetics of Mg. The addition of the oxides to Mg is also considered to facilitate nucleation by creating many defects on the surface and/or in the interior of Mg. The added oxides themselves may also act as active sites for the nucleation.

The order of high dehydriding rate and large quantity of hydrogen released for 60 min, from Fig. 2, is Mg–10MnO, Mg–10Fe_2O_3, Mg–10Cr_2O_3, Mg–10SiO_2, and the pure Mg, which is very different from the order of the particle size from Fig. 3. This shows that the rate-controlling step in the dehydriding reaction of magnesium hydride is other than

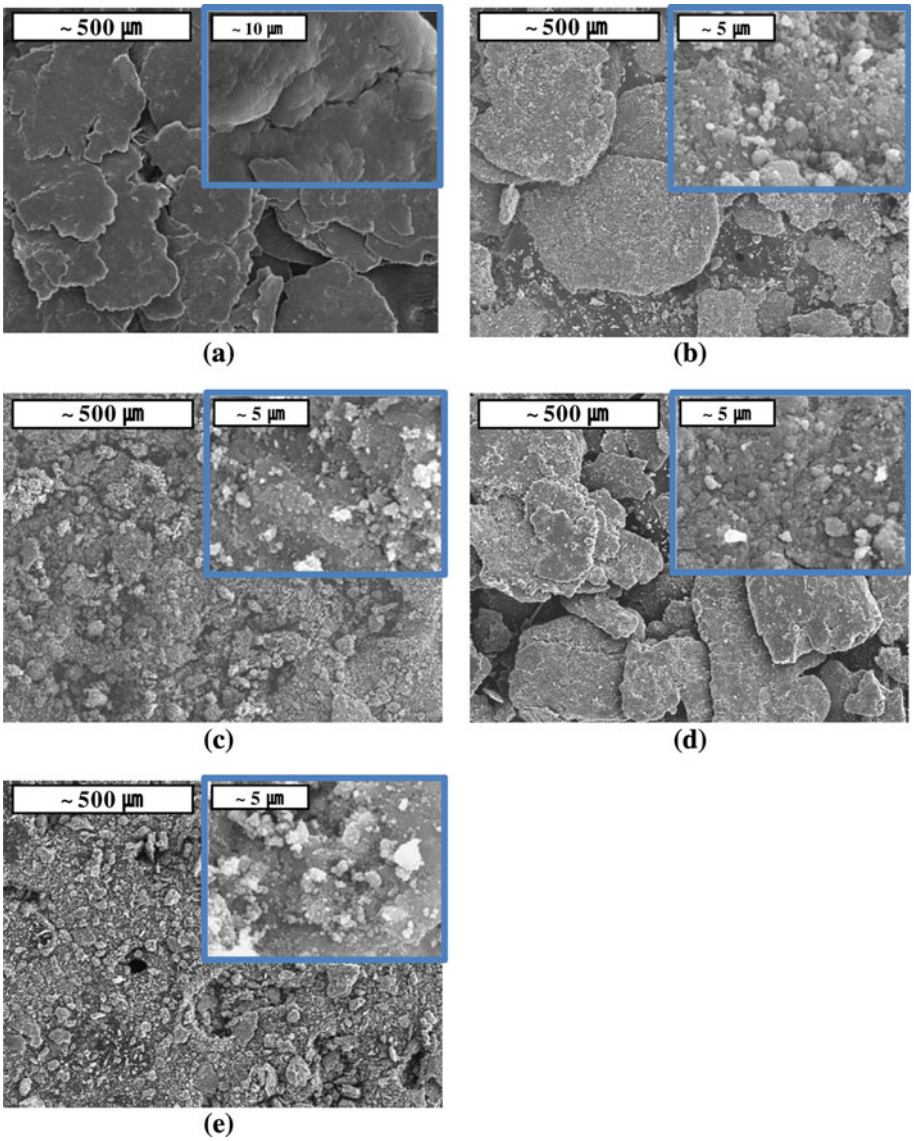

Fig. 3 Microstructures of the samples prepared by RMG of Mg with oxides; **a** pure Mg, **b** Mg–10MnO, **c** Mg–10Cr_2O_3, **d** Mg–10SiO_2, and **e** Mg–10Fe_2O_3

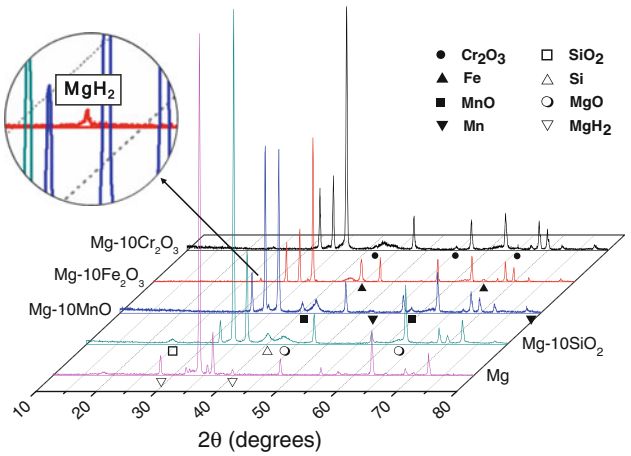

Fig. 4 XRD patterns of the Mg–10oxide samples dehydrided at 593 K for 3 h after activation

the diffusion of hydrogen through the growing magnesium–hydrogen α solid–solution layer.

Among Mg–10oxide samples, the Mg–10Cr_2O_3 sample has the highest hydriding rate. The Mg–10Cr_2O_3 sample absorbed 5.48 wt%H for 10 min and 5.72 wt%H for 60 min at 593 K, 1.2 MPa H_2, and desorbed 0.32 wt%H at 593 K, 0.1 MPa H_2 for 60 min. Its hydrogen-storage capacity was 6.38 wt% under 1.2 MPa H_2 at 593 K (from P–C–T curve). The activated Mg–10Fe_2O_3 sample absorbed 4.75 wt%H for 10 min and 5.55 wt%H for 60 min at 593 K, 1.2 MPa H_2. This sample desorbed 1.04 wt%H for 60 min at 593 K, 0.1 MPa H_2. Its hydrogen-storage capacity was 6.67 wt% under 1.2 MPa H_2 at 593 K (from P–C–T curve). From the view points of the hydriding and dehydriding rates and the cost of materials, the Mg–10Fe_2O_3 is considered a better Mg-based hydrogen-storage

material than the Mg–10Cr_2O_3. The addition of Ni to Mg increased greatly the hydriding and dehydriding rates of Mg [17, 18]. Because of that reason samples with the compositions of Mg–xFe_2O_3–yNi were prepared by RMG.

Figure 5 presents the variation of absorbed hydrogen quantity, H_a, versus time, t, curve at 593 K under 1.2 MPa H_2 with the activated Mg–xFe_2O_3–yNi sample. Mg–5Fe_2O_3–15Ni has the highest hydriding rate, followed in order by Mg–10Fe_2O_3, Mg–7.5Fe_2O_3–7.5Ni, Mg–10Fe_2O_3–5Ni, and Mg–5Fe_2O_3–5Ni. Mg–10Fe_2O_3 has the largest quantity of hydrogen absorbed for 60 min, followed in order by Mg–5Fe_2O_3–15Ni, Mg–7.5Fe_2O_3–7.5Ni, Mg–10Fe_2O_3–5Ni, and Mg–5Fe_2O_3–5Ni. Mg–5Fe_2O_3–15Ni stores 5.47 wt%H for 60 min at 593 K under 1.2 MPa H_2.

The variation of desorbed hydrogen quantity, H_d, versus time, t, curve at 593 K under 0.1 MPa H_2 with the activated Mg–xFe_2O_3–yNi sample is shown in Fig. 6. Mg–5Fe_2O_3–15Ni has the highest dehydriding rate, followed in order by Mg–7.5Fe_2O_3–7.5Ni, Mg–10Fe_2O_3–5Ni, Mg–5Fe_2O_3–5Ni, and Mg–10Fe_2O_3. Mg–5Fe_2O_3–15Ni releases 5.42 wt%H for 15 min at 593 K under 0.1 MPa H_2.

Microstructure of Mg–5Fe_2O_3–15Ni after RMG is exhibited in Fig. 7. The sample contains two fractions of particles; one with very small size and another with larger particles size. The second fraction is formed by agglomeration of the small particles. The particles have defects and cracks.

Figure 8 shows the XRD patterns of Mg–5Fe_2O_3–15Ni after RMG, the Mg–5Fe_2O_3–15Ni dehydrided at 593 K for 3 h after activation, and Mg–10Fe_2O_3 after RMG. The peaks with no marks in Fig. 8b are those of Mg phase. The Mg–5Fe_2O_3–15Ni after RMG, and Mg–10Fe_2O_3 after RMG contain MgH_2 in addition to starting materials. The XRD patterns reveal that, after RMG, the MgH_2 phase is

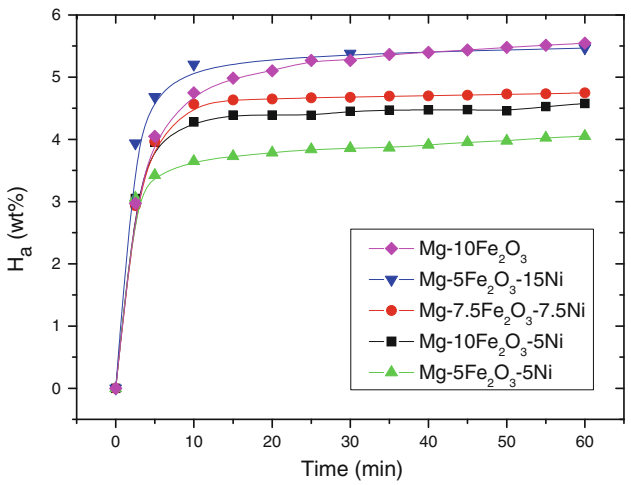

Fig. 5 Variation of absorbed hydrogen quantity, H_a, versus time, t, curve at 593 K under 12 bar H_2 with the activated Mg–xFe_2O_3–yNi sample

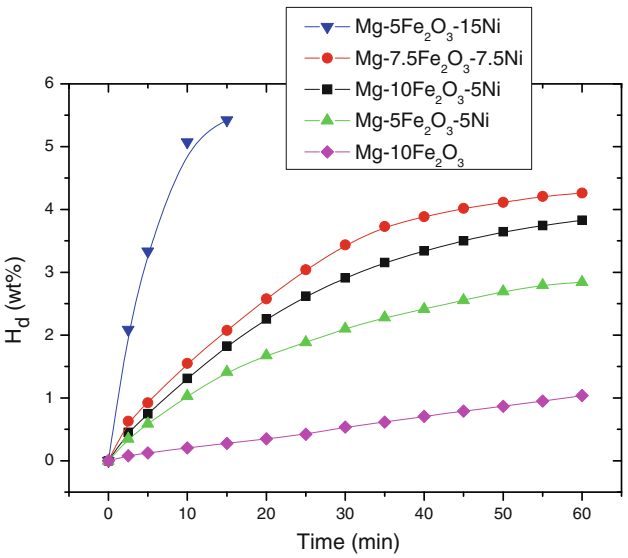

Fig. 6 Variation of desorbed hydrogen quantity, H_d, versus time, t, curve at 593 K under 1.0 bar H_2 with the activated Mg–xFe_2O_3–yNi sample

formed but the phase transformation of Fe_2O_3 does not occur. The MgH_2 peak in the sample Mg–5Fe_2O_3–15Ni after RMG is stronger than that in the sample Mg–10Fe_2O_3 after RMG, suggesting that Ni catalyzes the formation of MgH_2. The sample Mg–5Fe_2O_3–15Ni dehydrided at 593 K for 3 h contains Mg_2Ni and Fe phases, but the MgH_2 phase, which remained in the dehydridied Mg–10Fe_2O_3 sample (Fig. 4), was not observed. The Mg_2Ni phase is formed by the reaction of Mg with Ni during hydriding–dehydriding cycling, and Fe appears from the reduction of Fe_2O_3 by hydrogen.

The addition of Fe_2O_3 and Ni to Mg by the RMG shortens the diffusion distances through the reduction of the particle size of Mg and thus enhances the hydriding kinetics of Mg. It is also considered to facilitate nucleation by creating many defects on the surface and in the interior of Mg. The added Fe_2O_3 and Ni themselves may also act as active sites for the nucleation.

The rate-controlling step in the hydriding reaction of Mg_2Ni was reportedly the forced flow of hydrogen molecules through pores, interparticle channels or cracks of the particles [27]. Song [2] reviewed the kinetic studies of the hydriding and dehydriding reactions of magnesium; the hydriding and dehydriding reactions of magnesium are nucleation-controlled under certain conditions and progress by a mechanism of nucleation and growth, and the hydriding rates of magnesium are controlled by the diffusion of hydrogen through the growing magnesium–hydride layer. The ductile nature of Mg is considered to lead to the resistance of the decrease in the particle size whereas the particles of the intermetallic compound Mg_2Ni fragment

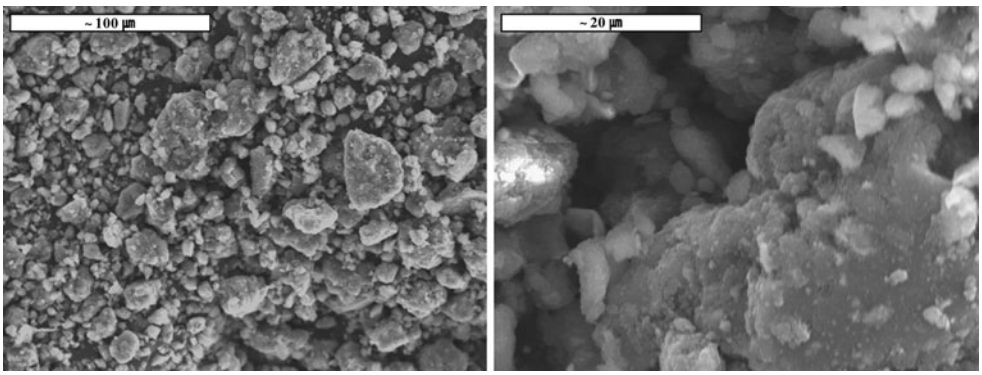

Fig. 7 Microstructure of Mg–5Fe_2O_3–15Ni after RMG

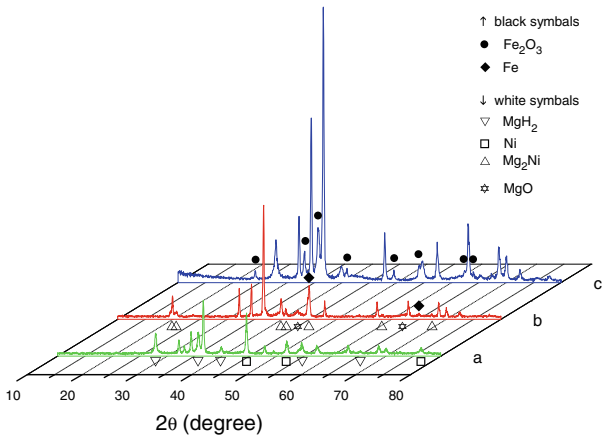

Fig. 8 XRD patterns of *a* Mg–5Fe_2O_3–15Ni after RMG, *b* Mg–5Fe_2O_3–15Ni dehydrided at 593 K for 3 h after activation, and *c* Mg–10Fe_2O_3 after RMG

easily thanks to its brittleness during RMG or hydriding–dehydriding cycling.

Ni forms the Mg_2Ni phase by a reaction with Mg during hydriding–dehydriding cycling. The Mg_2Ni phase has higher hydriding and dehydriding rates under similar conditions than Mg. For the Mg–$x$$Fe_2O_3$–$y$Ni samples, the hydriding and dehydriding rates and the quantity of hydrogen absorbed and released for 60 min increase as the content of Ni augments. The higher content of the Mg_2Ni phase with augmentation of Ni content could be related with these results.

The Fe formed from the reduction of Fe_2O_3 by hydrogen may act as the active sites for the chemisorptions of hydrogen molecules to atoms and combination of hydrogen atoms to molecules.

Conclusion

Taking into consideration the hydriding and dehydriding rates and the cost of materials, Fe_2O_3 prepared by spray conversion is an appropriate oxide additive to Mg. Mg–5 wt%Fe_2O_3–15 wt%Ni exhibited the best hydrogen-storage performance among the Mg–$x$$Fe_2O_3$–$y$Ni samples. It absorbed 5.47 wt%H under 1.2 MPa H_2 for 60 min and released 5.42 wt%H under 0.1 MPa H_2 for 15 min at 593 K. The addition of Fe_2O_3 and Ni to Mg by the RMG shortens the diffusion distances through the reduction of the particle size of Mg and thus enhances the hydriding kinetics of Mg. These additives are also considered to facilitate nucleation by creating many defects on the surface and in the interior of Mg. The added Fe_2O_3 and Ni themselves may also act as active sites for the nucleation. Ni forms the Mg_2Ni phase by a reaction with Mg during hydriding–dehydriding cycling. The Fe formed from the reduction of Fe_2O_3 by hydrogen may act as active sites for the chemisorptions of hydrogen molecules to atoms and combination of hydrogen atoms to molecules.

Acknowledgements This research was performed for the Hydrogen Energy R&D Center, one of the 21st Century Frontier R&D Programs, funded by the Ministry of Science and Technology of Republic of Korea. This paper was also supported by the selection of research-oriented professor (MyoungYoup Song) of Chonbuk National University in 2009.

References

1. Züttel A (2003) Mater Today 6(9):24
2. Song MY (1995) J Mater Sci 30:1343. doi:10.1007/BF00356142
3. Suryanarayana C (2001) Prog Mater Sci 46:1
4. Oelerich W, Klassen T, Bormann R (2001) J Alloys Compd 322:L5
5. Song MY, Bobet JL, Darriet B (2002) J Alloys Compd 340:256
6. Dehouche Z, Klassen T, Oelerich W, Goyette J, Bose TK, Schulz R (2002) J Alloys Compd 347:3195
7. Lee DS, Kwon IH, Bobet JL, Song MY (2004) J Alloys Compd 366:279
8. Barkhordarian G, Klassen T, Bormann R (2003) Scripta Mater 49:213
9. Barkhordarian G, Klassen T, Bormann R (2006) J Alloys Compd 407(1–2):249
10. Friedrichs O, Klassen T, Sanchez-Lopez JC, Bormann R, Fernandez R (2006) Scripta Mater 54(7):1293

11. Friedrichs O, Aguey-Zinsou F, Ares Fernandez JR, Sanchez-Lopez JC, Justo A, Klassen T, Bormann R, Fernández A (2006) Acta Mater 54(1):105
12. Dolci F, Di Chio M, Baricco M, Giamello E (2007) J Mater Sci 42(17):7180. doi:10.1007/s10853-007-1567-0
13. Aguey-Zinsou KF, Ares Fernandez JR, Klassen T, Bormann R (2006) Mater Res Bull 41(6):1118
14. Yavari R, LeMoulec A, de Castro FR, Deledda S, Friedrichs O, Botta WJ, Vaughan G, Klassen T, Fernandez A, Kvick Å (2005) Scripta Mater 52(8):719
15. Bogdanovic B, Spliethoff B (1987) Int J Hydrogen Energy 12(12):863
16. Imamura H, Sakasai N, Kajii Y (1996) J Alloys Compd 232(1–2): 218
17. Song MY, Ivanov EI, Darriet B, Pezat M, Hagenmuller P (1987) J Less Common Met 131:71
18. Bobet JL, Akiba E, Nakamura Y, Darriet B (2000) Int J Hydrogen Energy 25:987
19. Song MY, Baek SH, Bobet JL, Kwon SN, Hong SH (2009) J Mater Sci 44(18):4827. doi:10.1007/s10853-009-3736-9
20. Krozer A, Kasemo B (1989) J Phys Condens Matter 1(8):1533
21. Huot J, Tremblay ML, Schulz R (2003) J Alloys Compd 356–357:603
22. Imamura H, Kusuhara M, Minami S, Matsumoto M, Masanari K, Sakata Y, Itoh K, Fukunaga T (2003) Acta Mater 51(20):6407
23. Berlouis LEA, Honnor P, Hall PJ, Morris S, Dodd SB (2006) J Mater Sci 41(19):6403. doi:10.1007/s10853-006-0732-1
24. Grigorova E, Khristov M, Khrussanova M, Peshev P (2008) J Mater Sci 43(15):5336. doi:10.1007/s10853-008-2779-7
25. Khrussanova M, Mandzhukova T, Grigorova E, Khristov M, Peshev P (2007) J Mater Sci 42(10):3338. doi:10.1007/s10853-006-0586-6
26. Song MY, Hong SH, Kwon IH, Kwon SN, Park CG, Bae JS (2005) J Alloys Compd 398(1–2):283
27. Song MY, Pezat M, Darriet B, Lee JY, Hagenmuller P (1986) J Mater Sci 21:346. doi:10.1007/BF01144743